

# Inconsequence of Galaxy Major Mergers in Driving Star Formation at $z > 1$ : Insights from Cosmological Simulations

Renyue Cen<sup>1</sup>

## ABSTRACT

Utilizing a *high-resolution* ( $114h^{-1}\text{pc}$ ) adaptive mesh-refinement cosmological galaxy formation simulation of the standard cold dark matter model with a *large* (2000-3000 galaxies with stellar mass greater than  $10^9 M_\odot$ ) *statistical* sample, we examine the role of major mergers in driving star formation at  $z > 1$  in a cosmological setting, after validating that some of the key properties of simulated galaxies are in reasonable agreement with observations, including luminosity functions, SF history, effective sizes and damped Lyman alpha systems. We find that major mergers have a relatively modest effect on star formation, in marked contrast to previous idealized merger simulations of disk galaxies that show up to two orders of magnitude increase in star formation rate. At  $z = 2.4 - 3.7$ , major mergers tend to increase the specific star formation rate by 10 – 25% for galaxies in the entire stellar mass range  $10^9 - 10^{12} M_\odot$  probed. Their effect appears to increase with decreasing redshift, but is capped at 60% at  $z = 1.4 - 2.4$ . Two factors may account for this modest effect. First, SFR of galaxies not in major mergers are much higher at  $z > 1$  than local disk galaxy counterparts. Second, most galaxies at  $z > 1$  have small sizes and contain massive dense bulges, which suppress the merger induced structural effects and gas inflow enhancement. Various other predictions are also made that will provide verifiable tests of the model.

*Subject headings:* Methods: numerical, Galaxies: formation, Galaxies: evolution, Galaxies: interactions, intergalactic medium

## 1. Introduction

Simulations of major gas-rich disk galaxy mergers have provided quantitative insights to gas inflows and central starbursts under idealized conditions (e.g., Barnes & Hernquist 1996; Mihos & Hernquist 1996; Hopkins et al. 2006). These simulations have laid the foundation of the theoretical framework for almost all contemporary mainstream interpretations of observed extreme starbursting galaxies, namely, the ultraluminous infrared galaxies (ULIRGs),

---

<sup>1</sup>Princeton University Observatory, Princeton, NJ 08544; cen@astro.princeton.edu

as well as of the formation of supermassive black holes (e.g., Di Matteo et al. 2005). This framework is appealing, because almost all observed ULIRGs in the local universe either are directly seen merging or apparently show signs of mergers (at least some significant interactions) (e.g., Joseph & Wright 1985; Sanders et al. 1988; Duc et al. 1997; Lutz et al. 1998) and at least some luminous quasars live in galaxies under strong interactions (e.g., Bahcall et al. 1997). What is known but not sufficiently stressed in the relevant context is that the local universe is very different from the younger one at  $z > 1$  when star formation was much more intensive. As an example, a typical Lyman Break Galaxy (LBG) several times less massive than our own Galaxy has a star-formation rate (SFR) that is about ten times that of the Galaxy (e.g., Steidel et al. 2003). Moreover, minor mergers and close interactions between galaxies are expected to be much more frequent at high redshift that, cumulatively, may have important effects. Furthermore, there are significant structural differences between local galaxies and those at high redshift in that high redshift galaxies are more compact in size and the majority of massive quiescent galaxies that have been measured appear to have dense bulges (e.g., Lowenthal et al. 1997; Daddi et al. 2005; Trujillo et al. 2006b,a; Toft et al. 2007; Longhetti et al. 2007; Buitrago et al. 2008; Cimatti et al. 2008; van Dokkum et al. 2009; Cappellari et al. 2009; van de Sande et al. 2011). Therefore, our current physical interpretation of extreme galaxy events that is obtained based on linking local observations with substantially idealized major galaxy merger simulations may not pertain to the high redshift universe in general.

In this work we examine theoretically, in a cosmological setting, the role of major mergers in driving star formation in the redshift range  $z > 1$ , utilizing a large-scale high-resolution galaxy formation simulation. At each redshift from  $z = 1.4$  to  $z = 3.7$  the simulation contains 2000 – 3000 galaxies with stellar mass greater than  $10^9 M_\odot$  resolved at better than  $114h^{-1}\text{pc}$ . Detailed merger histories of galaxies are tracked and (binary) major mergers, defined to be those of stellar mass ratios greater than  $1/3$ , are examined in comparison to those that do not experience major mergers. We find that for galaxies with SFR in the range  $1 - 1000 M_\odot/\text{yr}$  and the stellar mass range  $M_{\text{star}} = 10^9 - 10^{12} M_\odot$  examined, major mergers, on average, yield a modest, fractional boost of  $0 - 60\%$  in specific SFR; we do not find two orders of magnitude increase in SFR found in previous merger simulations of disk galaxies (e.g., Mihos & Hernquist 1996). We show that the properties of simulated galaxies are in reasonable agreement with observations and give a physical explanation of the results. Additional predictions are provided to further test the model. The outline of this paper is as follows. In §2 we detail our simulation (§2.1) and galaxy catalogs (§2.2). Results are presented in §3, followed by §4 that gives a physical explanation of the results. Conclusions are given in §5.

## 2. Simulations

### 2.1. Hydrocode and Simulation Parameters

We perform cosmological simulations with the adaptive mesh refinement (AMR) Eulerian hydro code, Enzo (Bryan & Norman 1999; Joung et al. 2009). First we ran a low resolution simulation with a periodic box of  $120 h^{-1}\text{Mpc}$  on a side. We identified a region centered on a cluster of mass of  $\sim 2 \times 10^{14} M_{\odot}$  at  $z = 0$ . We then resimulate with high resolution of the chosen region embedded in the outer  $120 h^{-1}\text{Mpc}$  box to properly take into account large-scale tidal field and appropriate boundary conditions at the surface of the refined region. This simulation box is the same region as the “C” run in (Cen 2011b). The refined region for “C” run has a size of  $21 \times 24 \times 20 h^{-3}\text{Mpc}^3$ . The initial condition in the refined region has a mean interparticle-separation of  $58 h^{-1}\text{kpc}$  comoving, dark matter particle mass of  $1.3 \times 10^7 h^{-1} M_{\odot}$ . The refined region is surrounded by three layers (each of  $\sim 1 h^{-1}\text{Mpc}$ ) of buffer zones with particle masses successively larger by a factor of 8 for each layer, which then connects with the outer root grid that has a dark matter particle mass  $8^4$  times that in the refined region.

We choose the mesh refinement criterion such that the resolution is always better than  $114 h^{-1}\text{pc}$  physical, corresponding to a maximum mesh refinement level of 13 at  $z = 0$ . The simulation includes a metagalactic UV background (Haardt & Madau 1996), and a model for shielding of UV radiation by neutral hydrogen (Cen et al. 2005). They also include metallicity-dependent radiative cooling (Cen et al. 1995). Our simulation also solves relevant gas chemistry chains for molecular hydrogen formation (Abel et al. 1997), molecular formation on dust grains (Joung et al. 2009) and metal cooling extended down to 10 K (Dalgarno & McCray 1972). Star particles are created in cells that satisfy a set of criteria for star formation proposed by Cen & Ostriker (1992). Each star particle is tagged with its initial mass, creation time, and metallicity; star particles typically have masses of  $\sim 10^6 M_{\odot}$ .

Supernova feedback from star formation is modeled following Cen et al. (2005). Feedback energy and ejected metal-enriched mass are distributed into 27 local gas cells centered at the star particle in question, weighted by the specific volume of each cell, which is to mimic the physical process of supernova blastwave propagation that tends to channel energy, momentum and mass into the least dense regions (with the least resistance and cooling). We allow the entire feedback processes to be hydrodynamically coupled to surroundings and subject to relevant physical processes, such as cooling and heating. The total amount of explosion kinetic energy from Type II supernovae for an amount of star formed  $M_*$  with a Chabrier IMF is  $e_{SN} M_* c^2$  (where  $c$  is the speed of light) with  $e_{SN} = 6.6 \times 10^{-6}$ . Taking into account the contribution of prompt Type I supernovae, we use  $e_{SN} = 1 \times 10^{-5}$  in our simulation. Observations of local starburst galaxies indicate that nearly all of the star formation produced kinetic energy is used to power galactic superwinds (e.g., Heckman 2001).

Supernova feedback is important primarily for regulating star formation and for transporting energy and metals into the intergalactic medium. The extremely inhomogeneous metal enrichment process demands that both metals and energy (and momentum) are correctly modeled so that they are transported in a physically sound (albeit still approximate at the current resolution) way. The kinematic properties traced by unsaturated metal lines in DLAs are extremely tough tests of the model, which is shown to agree well with observations (Cen 2010). As we will show below, the properties of galaxies produced in the simulation resemble well observed galaxies, within the limitations of finite resolution.

We use the following cosmological parameters that are consistent with the WMAP7-normalized (Komatsu et al. 2010)  $\Lambda$ CDM model:  $\Omega_M = 0.28$ ,  $\Omega_b = 0.046$ ,  $\Omega_\Lambda = 0.72$ ,  $\sigma_8 = 0.82$ ,  $H_0 = 100h\text{kms}^{-1}\text{Mpc}^{-1} = 70\text{kms}^{-1}\text{Mpc}^{-1}$  and  $n = 0.96$ .

## 2.2. Simulated Galaxy Catalogs

We identify galaxies in our high resolution simulation using the HOP algorithm (Eisenstein & Hu 1999), operated on the stellar particles, which is tested to be robust and insensitive to specific choices of concerned parameters within reasonable ranges. Satellites within a galaxy are clearly identified separately. The luminosity of each stellar particle at each of the Sloan Digital Sky Survey (SDSS) five bands is computed using the GISSEL stellar synthesis code (Bruzual & Charlot 2003), by supplying the formation time, metallicity and stellar particle mass. Collecting luminosity and other quantities of member stellar particles, gas cells and dark matter particles yields the following physical parameters for each galaxy: position, velocity, total mass, stellar mass, gas mass, mean formation time, mean stellar metallicity, mean gas metallicity, star formation rate, luminosities in five SDSS bands (and various colors) and others.

We create catalogs of galaxies from  $z = 1.4$  to  $z = 3.7$  with an increment of  $\Delta z = 0.05$ . We track the merger history of each galaxy in this redshift span. There are two different ways to define major mergers. First, a theoretical one where we identify the merger time as that when two galaxies with a stellar mass ratio greater than 1/3 are fully integrated into one with no identifiable separate stellar peaks. Second, an observational one where a major merger is defined to be that where a galaxy has a neighbor galaxy with a stellar mass greater than 1/3 its mass at a lateral distance smaller than 40kpc proper. Both will be used in subsequent analysis. It is useful to state that the observationally-oriented definition does not always lead to a true merger of the usual sense, because either the two galaxies are a projected pair, or their merging time scale is much longer than the relevant dynamic time or the time before something else will have happened to the two concerned galaxies. Some informative comparisons or distinctions between the two will be made, when useful. We find that there are about 2000-3000 galaxies with stellar mass greater than  $10^9 M_\odot$  maximally resolved at

better than  $114h^{-1}\text{pc}$  at each redshift snapshot in the range  $z = 1.4 - 3.7$ , providing us with unprecedented statistical power.

In Cen (2011b) we show that galaxy luminosity functions for both UV and FIR selected galaxies can be self-consistently produced by the simulation. This, in combination with other, independent tests of the simulation, including the properties of the damped Lyman alpha systems (Cen 2010), strongly indicates a range of applicability of our simulation to complex systems, including galaxies at sub-kpc ISM scales. This validation of the simulation results is critical and allows us, with significant confidence, to perform the particular analysis here with respect to effects of major mergers.

### 3. Results

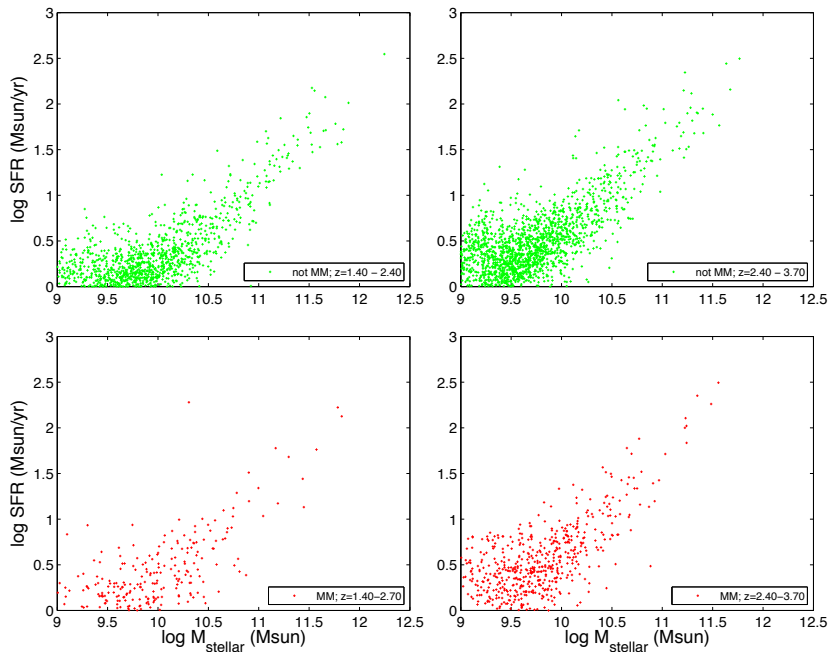


Fig. 1.— places each galaxy as a plus symbol in the SFR-stellar mass plane for non major merger galaxies in the redshift range  $z = 1.4 - 2.4$  (top left panel) and  $z = 2.4 - 3.7$  (top right panel). The corresponding ones for galaxies with major mergers are shown in the bottom panels. Here we adopt the observationally oriented definition of major mergers, i.e., pairs of stellar mass ratio greater than  $1/3$  and projected separation less than  $40\text{kpc}$ . Only a small percentage of randomly selected galaxies is shown.

Figure 1 shows scatter plots between SFR and stellar mass for galaxies that do not have ongoing major mergers (top two panels), compared to those that are ongoing major mergers (bottom two panels). Under visual inspection we see that there is no major discernible difference between galaxies that do and do not experience major mergers in the redshift

range examined for the entire range of stellar mass or SFR. It is noticeable that the number of galaxies that are major mergers is a minor fraction of all galaxies at any stellar mass or SFR.

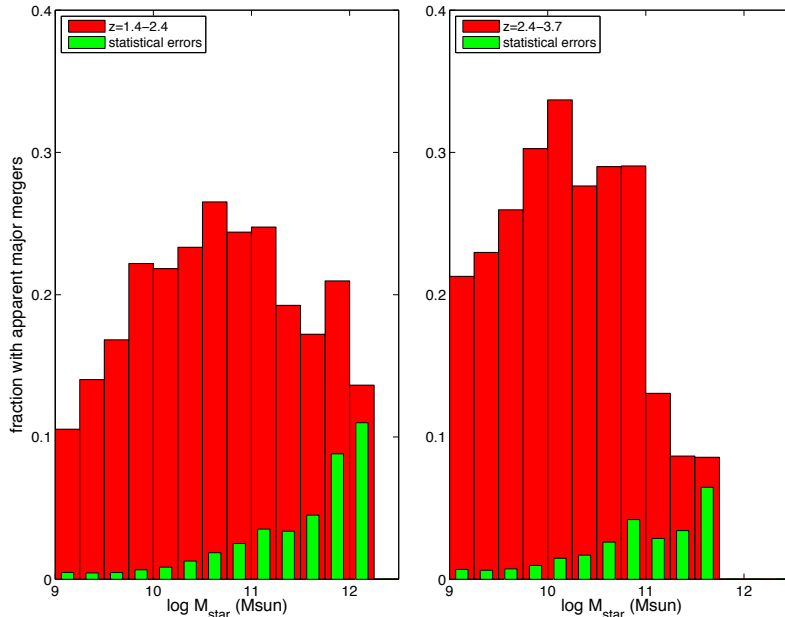


Fig. 2.— shows the fraction of galaxies that are in major merger as a function of stellar mass (red histograms) at  $z = 1.4 - 2.4$  (left panel) and  $z = 2.4 - 3.7$  (right panel). The statistical errors are shown as green histograms. We use the observationally oriented definition of major mergers, i.e., pairs of stellar mass ratio greater than  $1/3$  and projected separation less than  $40\text{kpc}$ .

Figure 2 shows the fraction of galaxies that are in major merger as a function of stellar mass with the observational definition. We note that the major merger fraction at the low stellar mass ( $< 10^{11} M_{\odot}$ ) is substantially overestimated due to the adopted definition, because many satellite galaxies within the virial radius of large galaxies are “mis-identified” as major mergers in this case. In fact, many of these satellite galaxies do not ever merge with one another directly in a binary fashion, as will be shown below in Figure 3. The fraction of major mergers at the high stellar mass end does not significantly suffer from this “projection” effect. We see that for galaxies with stellar mass in the range  $10^{11} - 10^{12} M_{\odot}$  major merger galaxies make up about  $10 - 20\%$  of *all galaxies* in that mass range.

The results on major merger fractions shown in Figure 2 (and Figure 4 below) are based on the observational definition of major mergers. It is useful to distinguish that from the theoretical one, where the latter is based on the actual merger events rather than pairs within some projected distance. Figure 3 shows the theoretical merger rate, defined to be the number of major mergers per unit redshift, as a function of galaxy stellar mass for galaxies

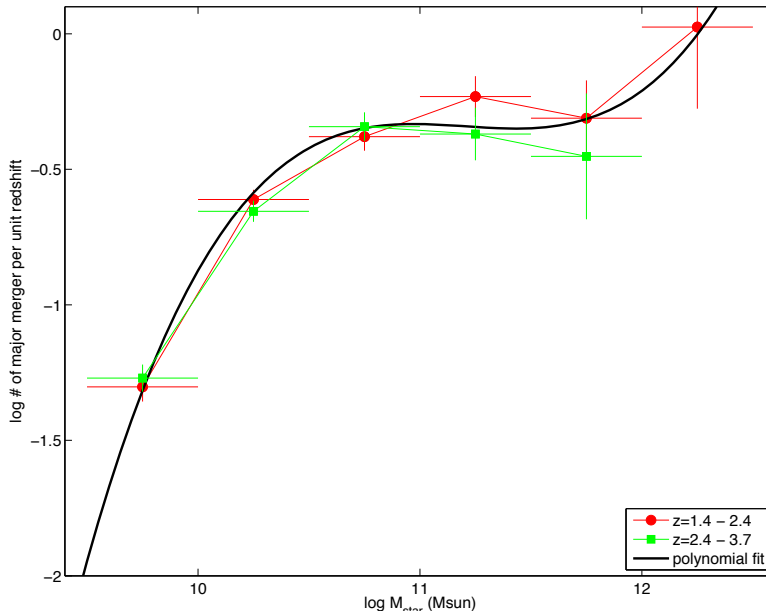


Fig. 3.— shows the merger rate (=number of major mergers per unit redshift) as a function of galaxy stellar mass for galaxies at  $z = 1.4$  (red dots) and  $z = 2.4$  (green squares). Here a merger is more physically based definition, an event where two galaxies of the stellar mass ratio greater than  $1/3$  physically merge.

at  $z = 1.4$  (red dots) and  $z = 2.4$  (green squares), respectively. We see that the actual merger rate is roughly constant at  $\sim 0.3 - 0.5$  per unit redshift for the stellar mass range  $M_{\text{star}} = 10^{10.5} - 10^{12} M_{\odot}$ . At  $M_{\text{star}} > 10^{12} M_{\odot}$  there is hint for a significant upturn in merger rate, albeit with less statistical certainty due to a small number of such massive galaxies in the simulation. Nevertheless, such an upturn would be consistent with the expectation that the central cD galaxies may experience more major mergers due to dynamical inspiral of satellites. This is also consistent with the apparent difference seen in Figure 3 between galaxies at  $z = 1.4 - 2.4$  (red) and galaxies at  $z = 2.4 - 3.7$  (green) in that the upturn is absent in the higher redshift range, because of the absence of large galaxies at that redshift range in the given simulation box. If the simulation box were large enough to contain cD-like galaxies at that higher-redshift range, we expect to see the same upturn.

The downturn at  $M_{\text{star}} < 10^{10.5} M_{\odot}$  of the merger rate is still more dramatic. We see a decrease of merger rate by a factor of  $\sim 10$  from  $M_{\text{star}} = 10^{10.5} M_{\odot}$  to  $M_{\text{star}} = 10^{9.5} M_{\odot}$ . This should be compared to about a factor of  $1.2 - 1.7$  drop seen in Figure 2 across the mass range. This shows that the vast majority of galaxies of mass  $M_{\text{star}} \leq 10^{10} M_{\odot}$  that are seen in close proximity ( $< 40$  kpc) with other galaxies of comparable masses are in fact do not end up in binary major mergers. In Cen (2011b) we show that the simulation reproduces observed luminosity functions in the concerned redshift range, indicating that the simulation is “complete” down to about a galaxy stellar mass of  $\sim 10^9 M_{\odot}$ . Thus, the results for the range of galaxy stellar mass shown here is reliable. A plausible physical explanation for the sharp downturn at the low mass end may be that most satellite galaxies just zoom around

and never merge with their fellow satellite galaxies rather they dynamically spiral in to merge with the primary galaxy or remain as satellites. A more detailed study focused on the demographics of mass accretion, including mergers, will be presented elsewhere. Here we present a third-order polynomial fit to the major merger rate,  $R$ , defined to be the number of major mergers per unit redshift:

$$\log R = 0.34(\log M_{\text{star}} - 11)^3 - 0.21(\log M_{\text{star}} - 11)^2 - 0.013(\log M_{\text{star}} - 11) - 0.33, \quad (1)$$

shown as the solid black curve in Figure 3, where  $M_{\text{star}}$  is in solar masses.

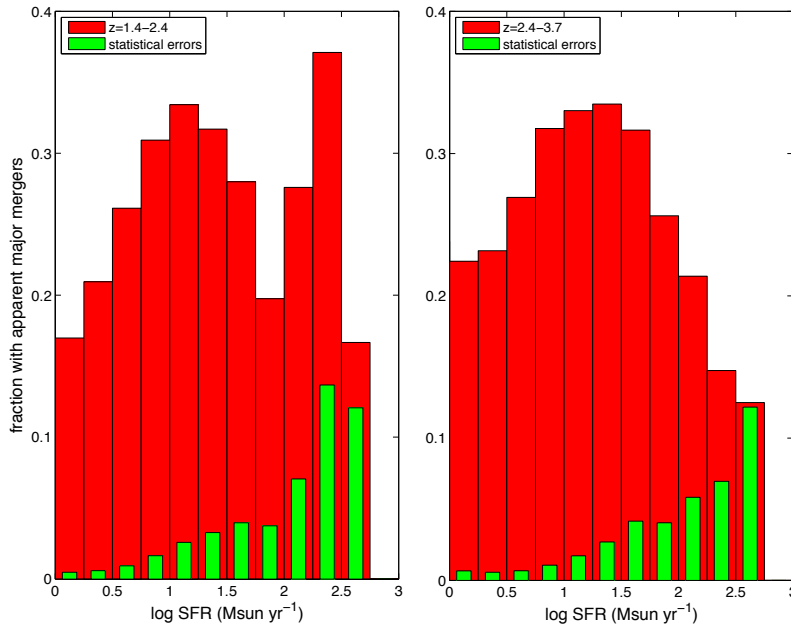


Fig. 4.— shows the fraction of galaxies that are in major merger as a function of SFR (red histograms) at  $z = 1.4 - 2.4$  (left panel) and  $z = 2.4 - 3.7$  (right panel). The statistical errors are shown as green histograms. We use the observationally oriented definition of major mergers, i.e., pairs of stellar mass ratio greater than  $1/3$  and projected separation less than  $40\text{kpc}$ .

Figure 4 shows the fraction of galaxies that are in major merger as a function of SFR. Similar to Figure 2, the actual major merger fraction at the low SFR end shown is overestimated, given the observational definition used. The major merger rate at the high SFR end, at  $\text{SFR} \geq 200 M_{\odot} \text{ yr}^{-1}$ , is less affected and the simulation shows that one should expect to see  $10 - 40\%$  of these high SFR galaxies to be in apparent major mergers. This fraction is consistent with the observed upper bound of  $57\%$  ( $8/14$ ) for the submillimeter galaxy (SMGs) sample of Tacconi et al. (2006) at  $z = 2 - 3.4$  that show a double-peaked profile in the CO  $3-2/4-3$  emission. Of this observed fraction of SMGs in major mergers, a fraction of it may be due to orbital motion of emitting gas in a disk configuration or some other configurations instead of major mergers. We predict that, when high spatial resolution become available with the upcoming ALMA mission, *the fraction due to major mergers should be in the range  $10 - 40\%$* , if our model is correct. For star-forming galaxies of  $\text{SFR} \leq 200 M_{\odot} \text{ yr}^{-1}$

at  $z = 1.4 - 3.7$ , we also predict that the major merger fraction should fall in the range of  $15 - 35\%$ . Recall that here we use the observationally oriented definition of major mergers, i.e., pairs of stellar mass ratio greater than  $1/3$  and projected separation less than  $40\text{kpc}$ .

To provide further tests of our model predictions, Figure 5 shows the probability distribution functions (PDFs) of the projected separation ( $r_p$ ) of major mergers at  $z = 1.4 - 2.4$  (top panels) and  $z = 2.4 - 3.7$  (bottom panels) for two subgroups of galaxies of  $\text{SFR} = 10 - 100 M_\odot \text{ yr}^{-1}$  (left panels) and  $\text{SFR} > 100 M_\odot \text{ yr}^{-1}$  (right panels), respectively. We find that the PDFs are reasonably fit with a single cored powerlaw of the following form:

$$\text{PDF}(r_p) dr_p \propto (r_c + r_p)^{-3/4} dr_p, \quad (2)$$

where the projected separation  $r_p$  and core size  $r_c$  are in physical kpc. The black curves shown in Figure 5 have  $r_c = 1$ , although it is not stringently constrained. The simple powerlaw fits are quite good, in contrast to gaussian or exponential forms that are found to provide poor fits. The found slope of  $-3/4$  in the PDF suggests that the three-dimensional distribution around each star-forming galaxy of other galaxies of comparable SFR approximately follows a powerlaw of a slope of  $-2.75$ . Details of this and other related clustering issues of galaxies will be presented elsewhere.

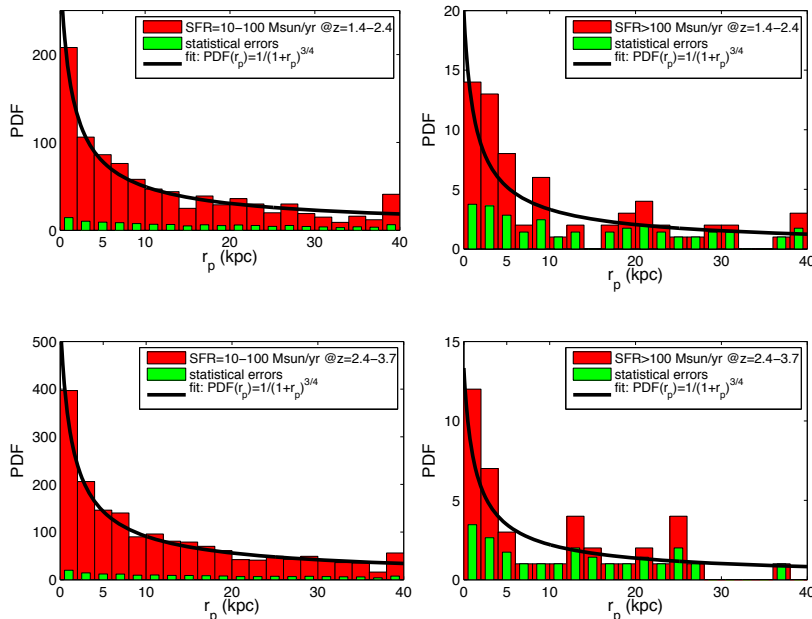


Fig. 5.— shows the probability distribution functions (PDF) of the projected separation ( $r_p$ ) of major mergers at  $z = 1.4 - 2.4$  (two upper panels) and  $z = 2.4 - 3.7$  (two bottom panels), respectively. The left panels are for star-forming galaxies of  $\text{SFR} = 10 - 100 M_\odot \text{ yr}^{-1}$  and the right panels for star-forming galaxies of  $\text{SFR} > 100 M_\odot \text{ yr}^{-1}$ . The red histograms are the PDFs and the green histograms the statistical errors at each bin. The black curves show a power fit described by Eq 2.

The top panel of Figure 6 shows the mean SFR as a function of galaxy stellar mass, separately, for galaxies that are in major mergers and galaxies that are not in major mergers.

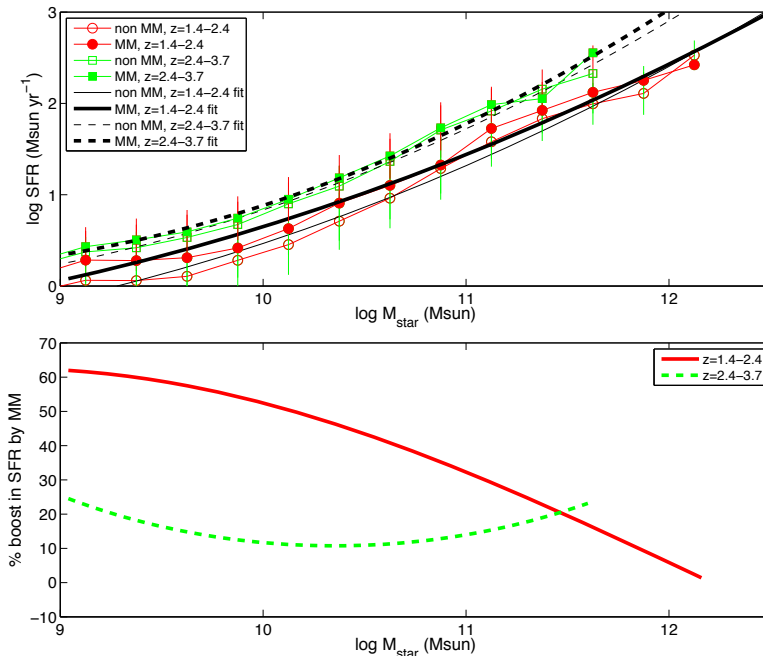


Fig. 6.— Top panel: the mean SFR of galaxies at a given stellar mass for galaxies that are in major mergers (red solid dots) and not in major mergers (red open dots) at  $z = 1.4 - 2.4$ . The corresponding ones at  $z = 2.4 - 3.7$  are shown in green squares. The errorbars show the dispersion around the mean. The thin and thick dashed curves are the best second-order polynomial fits to the non major mergers and major mergers, respectively, at  $z = 1.4 - 2.4$ . The thin and thick solid curves are the best second-order polynomial fits to the non major mergers and major mergers, respectively, at  $z = 2.4 - 3.7$ . We use the observationally oriented definition of major mergers, i.e., pairs of stellar mass ratio greater than  $1/3$  and separation less than  $40\text{kpc}$ . Bottom panel: the ratio of fitted curves to the major merger and non-major-merger minus one for  $z = 1.4 - 2.4$  (red solid curve) and  $z = 2.4 - 3.7$  (green dashed curve), respectively. Visually the ratio of the fitted curves and the actual computed data points display comparable amplitudes.

The ratio of fitted curves for the galaxies with major mergers and those without major mergers minus one are shown in the bottom panel for  $z = 1.4 - 2.4$  (red solid curve) and  $z = 2.4 - 3.7$  (green dashed curve). We see that major mergers appear to experience very modest boost in SFR for galaxies at  $z = 2.4 - 3.7$ , at about  $10 - 25\%$  for the entire stellar mass range  $M_{\text{star}} = 10^9 - 10^{12} M_{\odot}$  probed. The overall strength of the boost due to major mergers appear to increase with decreasing redshift, when one compares the values at  $z = 1.4 - 2.4$  to those at  $z = 2.4 - 3.7$ , but remains at less than  $60\%$  across the entire mass range. It also appears that there may be a trend of a relatively larger boost of SFR due to major mergers for lower mass galaxies than for larger mass galaxies at  $z = 1.4 - 2.4$ . But we caution that the results in the bottom panel are somewhat sensitive to the exact fits; given that the fits do not exactly reproduce all the data points, one should be careful to not take the exact curves of the fits too literally. In any case, it is abundantly clear that we *do not see very large increase in SFR of a factor of two orders of magnitude* that are found in simulations of isolated major gas-rich spiral galaxy mergers (e.g., Mihos & Hernquist 1996).

In Figure 6 the modest boost in SFR due to major mergers is computed using the

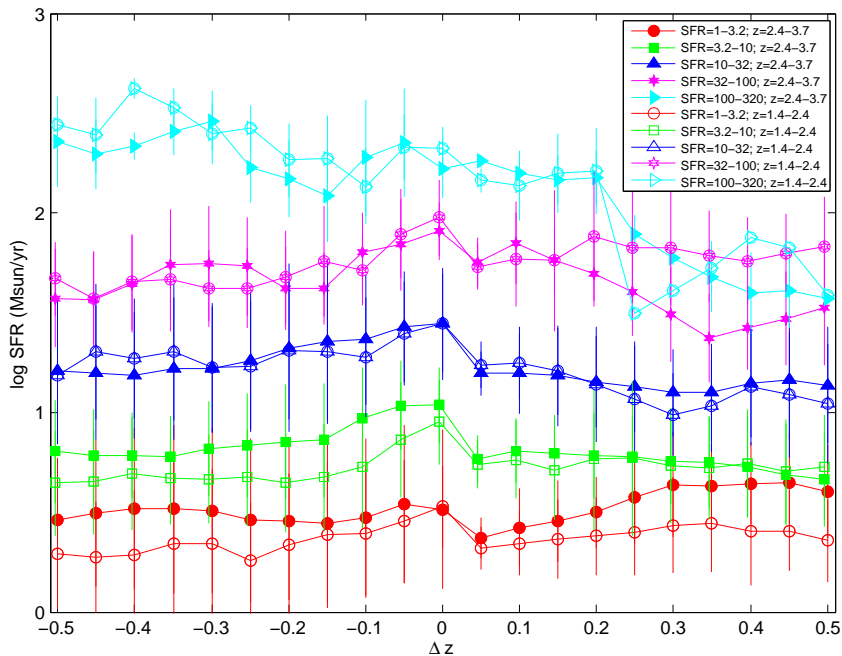


Fig. 7.— shows the history of the mean SFR as a function of time redshift  $\Delta z$  for five different subsets of galaxies with SFR at  $\Delta z = 0.05$  (i.e., prior to the merger event) equal to 1 – 3.2, 3.2 – 10, 10 – 32 and 32 – 100, 100 – 320  $M_{\odot} \text{ yr}^{-1}$ , respectively, separately for galaxies in the redshift range  $z = 1.4 - 2.4$  and  $z = 2.4 - 3.7$ . Dispersions on the means are shown as well.

observationally oriented definition of major mergers, i.e., pairs of stellar mass ratio greater than 1/3 and projected separation less than 40kpc. We now compute a similar quantity using the theoretical definition of major mergers where we identify the merger time as that when two galaxies are fully integrated into one with no identifiable separate stellar peaks. We follow the history of each galaxy and “stack” all major merger events centered at  $\Delta z = 0$ . Figure 7 shows the mean SFR history for galaxies at five given ranges of SFR, measured at  $\Delta z = 0.05$  (using a different redshift, say,  $\Delta z = 0.10$  or  $0.15$ , makes no material difference in the results). In a fashion that is consistent with the findings shown in Figure 6, we do not find any dramatic boost of SFR at the merger redshift and at  $|\Delta z| \leq 0.5$  for galaxies at  $\text{SFR} \leq 100 M_{\odot} \text{ yr}^{-1}$  in the redshift range  $z = 1.4 - 3.7$ . The  $1\sigma$  dispersion about the mean is about 1.5 – 3, roughly consistent with the range of SFR for each subset at  $\Delta z = 0.05$ ,

with a tendency that the dispersion is larger for lower SFR subsets. For the subset with the largest SFR ( $\geq 100 M_{\odot} \text{ yr}^{-1}$ ), however, there is a visually noticeable jump in SFR by a factor of  $\sim 2 - 5$  from  $\Delta z > 0.2$  to  $\Delta z < 0.2$ , hinting an intriguing possibility that a major merger event, not necessarily the final major merger moment, serves to “trigger” a very high SFR event. In other words, it suggests that some very high SFR galaxies, such as ULIRGs or SMGs, may be *initially* triggered by some major merger events. At the same time results in Figure 7 also suggest that the very high SFR ( $\geq 100 M_{\odot} \text{ yr}^{-1}$ ) galaxies remain at the elevated and upward trend for SFR following the merger event for a long period of time ( $\Delta z \sim 1$ ) that is much longer than the typical merger time scale. This has profound implications for the nature of ULIRGs and SMGs that will be addressed elsewhere.

#### 4. Physical Explanation of the Results

Both external gravitational and internal gravitational and hydrodynamic torques may drive gas inward. Externally, the tidal field from a companion during a galaxy merger, major or minor, gives rise to a non-axisymmetric gravitational potential. This induces a response of the disk material (Toomre & Toomre 1972), in particular its cold gas, stronger for prograde mergers. More broadly, tidal fields from interacting galaxies, which are not necessarily merging with one another, may drive gas inward. Internally, non-axisymmetric gravitational potentials, notably those sustained by stellar bars that are produced by secular evolution of sufficiently cold stellar disks under certain conditions or from other interactions, such as mergers, can also drive gas inward. A thorough study of torques due to gravitational and hydrodynamic processes to isolate the primary physical mechanisms governing the gas inflows in a cosmological setting will be performed in a larger study. Here we provide some physical insight for the results found, relying mainly on circumstantial but strong evidence.

Anecdotal evidence and visual examination of some galaxies suggest that chaotic gas inflows often result in mis-alignments of newly formed stellar disks with previous stellar disk/non-spherical bulges, and the orbital planes of infalling satellite stellar or gas clumps do not always have a fixed orientation. These processes cumulatively may be thought to create stellar distributions in the central regions that are dynamically hot, which, in turn, provides conditions that are unfavorable to secular formation of stellar bars. We check if this indeed is the case.

The left panel of Figure 8 shows axial ratios  $c/b$  versus  $b/a$ , where  $c < b < a$  are the semi-axes of an ellipsoid approximating the stellar distribution within  $r_e$  for galaxies with  $\text{SFR} \geq 10 M_{\odot} \text{ yr}^{-1}$  with major mergers (solid dots) and without (open circles) at  $z = 2$ . We see that the stellar distribution within  $r_e$  typically resembles an oblate spheroid with the half-height approximately equal to one half of that of the disk radius or more. For such hot stellar systems no barlike equilibria exist and no strong stellar bars would form

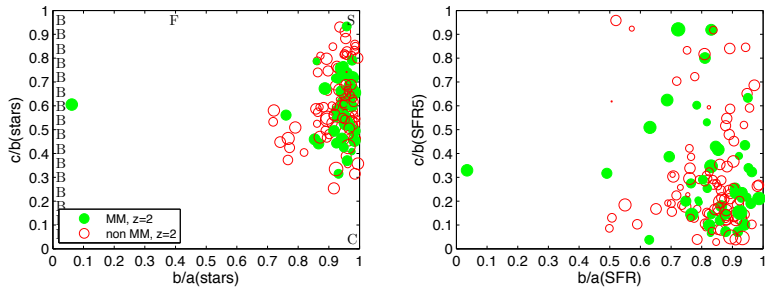


Fig. 8.— Left panel: shows axial ratios  $c/b$  versus  $b/a$ , where  $c < b < a$  are the semi-axes of an ellipsoid approximating the stellar distribution within  $r_e$  for galaxies with  $\text{SFR} \geq 10 M_\odot \text{yr}^{-1}$  with major mergers (solid dots) and those without (open circles) at  $z = 2$ . The symbol size in both panels is linearly proportional to the logarithm of its SFR. Several special locations are indicated by special letters: “B” for thin bars of various thickness, “S” for sphere, “C” for flat circular disk and “F” for American football. Right panel: shows the same but for SFR density distribution within the radius of 50% SFR.

secularly (e.g., Ostriker & Peebles 1973). Indeed, we do not find any instance of thin stellar bars that would occupy locations near the left y-axis; the one instance seen is in fact a close merging pair, which, when approximated as an ellipsoid by our code, shows up as a thin bar. The right panel of Figure 8 shows the same for SFR density, which shows that ongoing star formation in the central region for the majority of galaxies at  $z \geq 1$  takes place on a relatively thin disk of typical height-to-radius ratio of  $0.1 - 0.3$ , with some ratios reaching as low as  $0.03$ , approaching our resolution limit of  $\sim 100\text{pc}$ . It is clear, however, the relatively thick stellar bulges seen in the left panel of Figure 8 are very well resolved and little affected by resolution effects. The number of stellar particles within  $r_e$  for mass in the range  $10^9 - 10^{12} M_\odot$  are typically  $N \sim 10^{3.5} - 10^{6.5}$  and the two-body relaxation time is roughly  $t_r \approx (N/50)t_c$  (e.g., Steinmetz & White 1997), where  $t_c$  is the orbital period at  $r_e$ . For a galaxy with  $M_{\text{star}} = 10^{10} M_\odot$  ( $N \sim 10^{4.2}$  within  $r_e$ ) and  $r_e \sim 0.5\text{kpc}$  (see Figure 11 below) the relaxation heating time is estimated to be  $\sim 1 \times 10^{10}\text{yr}$ . A typical galaxy with  $M_{\text{star}} = 10^{10} M_\odot$  corresponds to  $\text{SFR} \sim 10 M_\odot/\text{yr}$  at the relevant redshift range. Thus, we expect the two-body relaxation heating to be completely negligible for galaxies with  $\text{SFR} \geq 10 M_\odot/\text{yr}$ . This shows that the dynamically hot state of the central stellar bulges of the simulated galaxies is unlikely caused by numerical effects. In the left panel of Figure 8 we do not see significant difference between galaxies with major mergers and those without, indicating that major mergers do not appear to enhance formation of structures that resemble bars; this issue will be further examined below.

In the absence of strong stellar bars, can significant gas inflows still exist? Figure 9 shows the gas depletion time in central regions at  $r < 1\text{kpc}$  (left panel) and over the entire galaxy within the virial radius (right panel) for all galaxies with  $\text{SFR} \geq 10 M_\odot \text{yr}^{-1}$ . The right panel indicates that the gas depletion time over the entire galaxy is longer than its

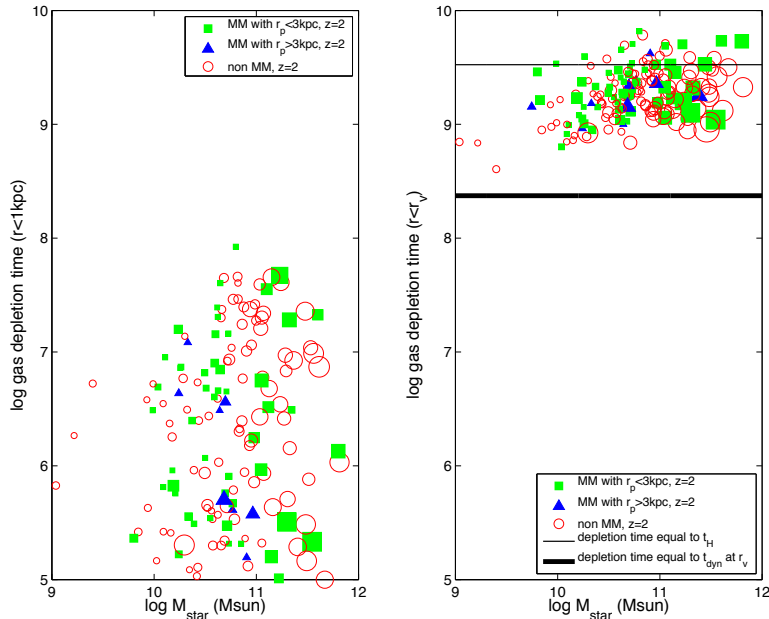


Fig. 9.— Left panel: gas depletion time within the central 1kpc region of galaxies at  $z = 2$  with  $\text{SFR} \geq 10 M_{\odot} \text{yr}^{-1}$ . Three types of galaxies are shown using different symbols: galaxies that are not undergoing major mergers are open circles, galaxies in major mergers with projected separation between the two galaxies less than 3kpc as squares and greater than 3kpc as triangles. Right panel: gas depletion time over the entire galaxy within the virial radius. The symbol size is linearly proportional to the logarithm of SFR. The thin and thick horizontal lines correspond to the Hubble time and dynamical time at virial radius at  $z = 2$ , respectively. Here the observational definition of major mergers is used.

dynamic time and comparable to the Hubble time. The gas depletion time in the central 1kpc region, however, is shorter at  $\leq 100 \text{Myrs}$ . The gas depletion time in the central region spans a wide range,  $0.1 - 100 \text{Myrs}$ , and there is no discernible difference between galaxies in major mergers (solid symbols) and those that are not (open symbols). Furthermore, there is no visible dependence of the depletion time in the central region on the separation of the two merging galaxies for those that are in major mergers. Examination of SF histories of individual galaxies indicate that the SFR are relatively steady and their durations are on the order of Hubble time, i.e., much longer than the gas depletion time scales of the central regions but comparable to the gas depletion time scales within the virial radii shown in Figure 9 (Figure 6 shows that for galaxies with mergers within  $\Delta z = 0.5$ ). This suggests that, irrespective of being in major mergers or not, gas inflows to the central regions appear to be ubiquitous; in other words, galaxies that are not in major mergers appear to be able to channel a sufficient amount of gas to fuel the star formation on time scales that are much longer than the gas depletion times in the central regions. The disparity in the gas depletion time scales of the central regions and between those and the overall star formation durations strongly imply that gas inflows, in general, are not smooth but in the form of clumps falling

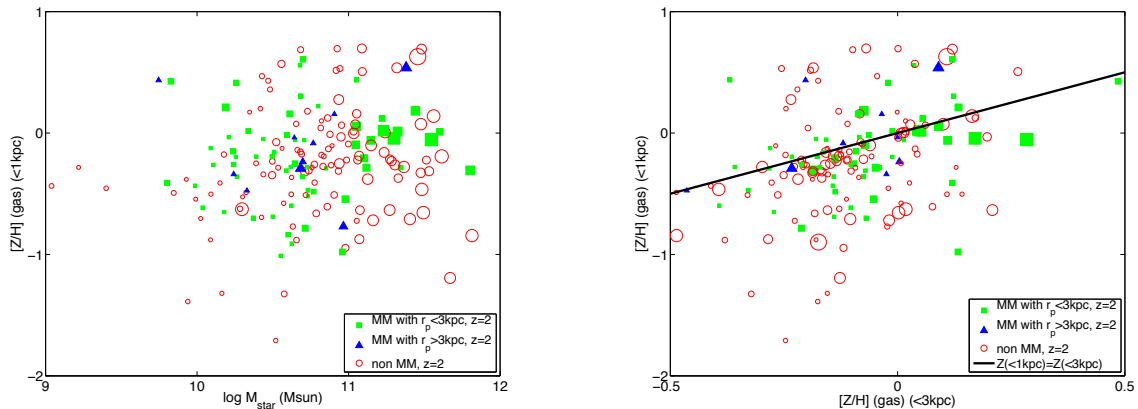


Fig. 10.— Left panel: the mean gas metallicity within the central 1kpc region as a function of galaxy stellar mass for galaxies with  $\text{SFR} \geq 10 M_{\odot} \text{yr}^{-1}$ . Three types of galaxies are shown using different symbols: galaxies that are not undergoing major mergers are open circles, galaxies in major mergers with projected separation between the two galaxies less than 3kpc as squares and greater than 3kpc as triangles. Right panel: the mean gas metallicity within the central 1kpc region as a function of the mean gas metallicity within the central 3kpc region galaxy stellar mass for galaxies with  $\text{SFR} \geq 10 M_{\odot} \text{yr}^{-1}$ . The symbol size in both panels is linearly proportional to the logarithm of its SFR.

in intermittently.

To further demonstrate that gas inflows towards the central regions are generally not caused by central non-spherical gravitational perturbations, the left panel of Figure 10 shows the mean gas metallicity in the central 1kpc region and the right panel shows the mean gas metallicity in the central 1kpc region as a function of the mean gas metallicity in the central 3kpc region, comparing galaxies with and without major mergers. From both panels we see that there is no visible difference in the metallicity of gas in the central regions between galaxies that are in major mergers and those that are not. It is seen that there is a relatively large span of mean gas metallicity in the central 1kpc region, from  $\sim -1.5$  to  $\sim 0.5$  for both types of galaxies, while the range shrinks to about  $-0.5$  to  $0.5$  within 3kpc for both types of galaxies. If non-spherical gravitational perturbations in the central regions were responsible for driving gas inward, they would be most effective for the gas in the immediate neighborhood. Consequently, if the central 1kpc region were just fed by gas driven inward from the immediate surroundings by internal non-spherical gravitational perturbations within, one would expect to see a higher gas metallicity in the central 1kpc than in the central 3kpc, since star formation rate is super-linear on gas density (the Schmidt-Kennicutt law) hence SFR density stronger in the 1kpc central region than in the 3kpc central region per unit gas. This expectation is not universally borne out for all galaxies in the simulation; on the contrary, the majority of galaxies lie below the  $Z(<1\text{kpc}) = Z(<3\text{kpc})$  line, and there exists low mean metallicity ( $Z < -0.5$ ) gas in the central 1kpc that is not seen in the mean metallicity within the central 3kpc. This is unambiguous evidence that a

significant amount of gas inflow is directly “parachuted in” (e.g., dynamical friction inspiral of gas clumps with or without dark matter halos, or infalling satellites on nearly radial orbits) or “channelled in” (e.g., clumpy cold streams) from large scales, not smooth gas from regions that immediately surround it, at least for a large fraction of galaxies. This is consistent with the implied intermittency of fueling seen in Figure 9. In any event, the results indicate that major mergers do not appear to form a distinct set of galaxies with respect to gas metallicity in the central regions.

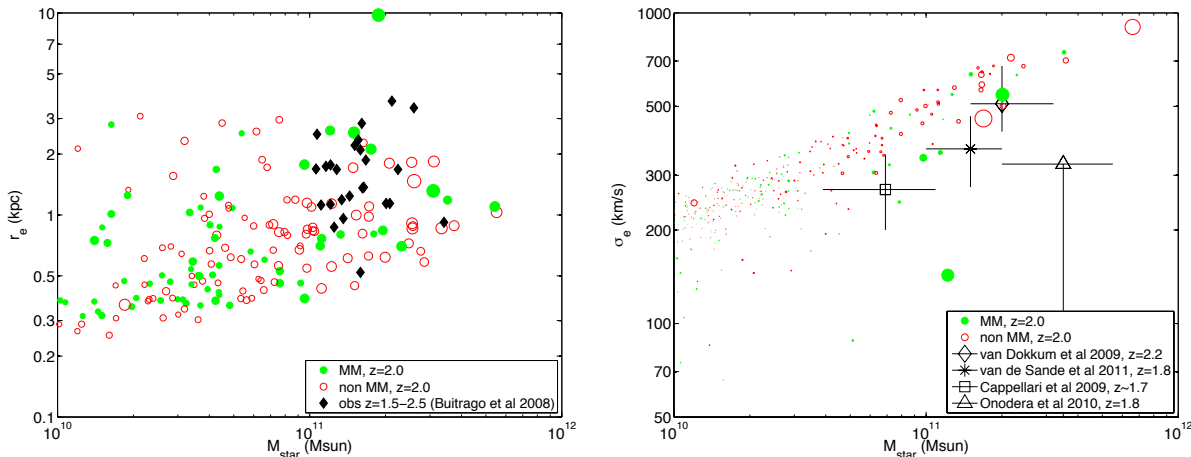


Fig. 11.— Left panel: the effective radii of galaxies in restframe V band (observed H band) versus the stellar masses for galaxies with major mergers (solid dots) and those without (open circles) at  $z = 2$ . Also shown as solid diamonds are the observations of Buitrago et al. (2008) for the subset of galaxies at  $z = 1.5 - 2.5$  observed in H band. The symbol size in the left panel is linearly proportional to the logarithm of SFR. Right panel: the relation between velocity dispersion (y axis) and dynamical mass (x axis) at  $r_e$ . The black diamond, star, square and triangle symbols with cross errorbars are the observational data for galaxies in the range range  $z = 1.7 - 2.2$  from van Dokkum et al. (2009), van de Sande et al. (2011), Cappellari et al. (2009) and Onodera et al. (2010), respectively. The symbol size in the right panel is linearly proportional to the SFR.

Mihos & Hernquist (1996) show that galaxy structure plays a dominant role in regulating gas inflows, which they find are generally driven by gravitational torques from the host galaxy, rather than the companion, in their major merger simulations. The lack of any significant merger induced effects appear at odds with their simulations at first instance. We attribute the difference primarily to the difference in the physical properties of galaxies between merger simulations and those in present cosmological simulation at  $z > 1$ . Specifically, as we will show shortly, most of galaxies in our simulation appear to have massive stellar bulges, whereas merger simulations with dramatic inflows seen during mergers start with pre-merger disk galaxies without massive stellar bulges. In fact, a subset of simulations by Mihos & Hernquist (1996) where the pre-merger galaxies have massive stellar bulges has already provided insight for the above apparent discrepancy: they note that dense bulges act to

stabilize galaxies against bar modes and have much diminished inflow enhancement.

In the left panel of Figure 11 we show the effective stellar radii in restframe V band of galaxies with  $\text{SFR} \geq 10 \text{ M}_{\odot} \text{ yr}^{-1}$  at  $z = 2$ , compared to observed galaxies also in restframe V band (observed H band). We see that the effective radii of most simulated galaxies at  $z = 2$  are in the range of  $0.5 - 2 \text{ kpc}$  for galaxies of stellar mass  $\geq 10^{11} \text{ M}_{\odot}$ , consistent with previous results (Joung et al. 2009; Naab et al. 2009), and are in reasonable agreement with observations. No dust obscuration is applied in the calculation so the computed radii are likely lower limits; if we had taken dust obscuration into account, we expect the agreement would still be better. The right panel of Figure 11 shows the 1-d velocity dispersion at the effective stellar radius as a function of stellar mass and we find that within the uncertainties the simulation results are in agreement with the observations, indicative of a self-consistency of the simulation results. The observed high value of central velocity dispersion (van Dokkum et al. 2009) was somewhat surprising initially based on an extrapolation of local elliptical galaxy properties, but now that additional observations have confirmed the earlier discovery and our simulations indicate that this is in fact in line with the theoretical expectation based on the cold dark matter model. There is one exception (Onodera et al. 2010) that shows a lower central velocity dispersion; our current statistics are insufficient to gauge this against our model one way or another. Although the simulation results and observations are statistically consistent with one another, enlarging both the simulation size and observed galaxy sample size may provide very useful constraints on physical processes that govern the formation of the bulges. If pressed, one might incline to conclude that there is a slight hint that the simulated galaxies are slightly smaller than the handful of observed galaxies, although the observed ones overlap and are statistically consistent with the simulated range in terms of velocity dispersion at a fixed stellar mass. Nonetheless, three effects may have caused slight overestimation of the velocity dispersions of simulated galaxies. First, no dust obscuration effect is taken into account. Second, no observational beam smearing effect is taken into account. Third, the simulated galaxies at a fixed stellar mass have a range in SFR, whereas the observed galaxies shown are thought to be quiescent; one might think that gas loss from aging or dying stars acts in the direction of enlarging stellar cores with aging stellar population due to adiabatic expansion related to mass loss that is known to be substantial.

To be prudent and conservative, we have purposely plotted the symbol size in the right panel of Figure 11 to be linearly proportional to the SFR to see if there is noticeable trend in SFR with core size/velocity dispersion. We see one case, the green solid dot at  $(1.3 \times 10^{11} \text{ M}_{\odot}, 150 \text{ km/s})$ , that has a SFR that may be a factor of a few higher than typical galaxies at around that mass. However, we also see galaxies to have higher SFR even though having much higher velocity dispersions, with or without major mergers. In any case, it appears that some of the noticeably high SFR galaxies are consistent with being randomly distributed with respect to  $\sigma_e$ . Thus, we conclude that there is no dramatic trend of SFR with

respect to  $\sigma_e$  at a fixed stellar mass in the range of  $\sigma_e$  that overlaps with observed values, save the one noted exceptions that is presently difficult to gauge statistically. This check suggests that our results are not hinged on our modeling of the size of the central stellar bulges being perfectly correct and are thus robust to possible small variations. Taking the evidence presented in the preceding four figures together a consistent physical picture emerges:

- Gravitational or hydrodynamic torques stemming from scales larger than the central regions containing most of the stars in the primary galaxy may play a fundamental role in transporting the necessary amount of gas to fuel the star formation in the central regions.

- A large portion of often metal-poor gas from large scales is directly transported into the central regions, possibly in the form of dynamical friction inspiraling gas clumps, infalling satellites on nearly radial orbits, or clumpy cold streams from large scales in an intermittent fashion.

- Significant gas inflows, not necessarily requiring major mergers, allow for formation of dense, compact, not-so-flat stellar bulges that are stable to bar formation.

- Major mergers of galaxies, most of which have dense bulges, do not dramatically enhance gas inflows and SFR or cause significant differences in gas properties in the central regions for galaxies at  $z \geq 1$ , in accord with earlier major mergers simulations of disk galaxies with massive bulges.

## 5. Conclusions

With high resolution and a physically sound treatment of relevant physical processes, our state-of-the-art, adaptive mesh-refinement Eulerian cosmological hydrodynamic simulations have reproduced well some key observables of the galaxy population as a whole (Cen 2010, 2011a,b), including galaxy luminosity functions at  $z = 0 - 3$ , galaxy color distribution at  $z = 0$ , the entire star formation history, and properties of damped Lyman alpha systems that we have so far examined. Here we study how major mergers affect star formation. The simulation contains about 2000–3000 galaxies with stellar masses in the range  $10^9 - 10^{12} M_\odot$  and resolved at better than  $114h^{-1}\text{pc}$  at  $z = 1.4 - 3.7$ , providing a good statistical sample to examine major mergers for a wide of range of galaxies in mass and SFR.

The most significant finding is that major mergers, on average, do not result in two orders of magnitude boost in SFR, as found in simulations of major mergers of gas-rich disk galaxies with idealized initial conditions. Rather, for the redshift range examined,  $z = 1.4 - 3.7$ , major mergers give rise to an average boost 0 – 60% in specific SFR for SFR in range of 1 – 1000  $M_\odot/\text{yr}$  examined. Two physical factors of cosmological origin that are not taken into account in isolated merger simulations may be responsible for the difference.

First, the central regions ( $\sim 1\text{kpc}$ ) of galaxies at  $z > 1$ , in the absence of major mergers, are being fed, in an intermittent fashion, with significant gas inflows. As a result, galaxies without major mergers at  $z > 1$  have much higher SFR than their lower redshift counterparts, a fact that is known observationally. We demonstrate that, at least for a significant fraction of galaxies, gas inflows to the central regions, often quite metal poor, originate from large scales (not smooth gas from the regions immediately surrounding the central region) possibly in the form of dynamical friction inspiraling gas clumps, infalling satellites on nearly radial orbits, or clumpy cold streams from large scales. We suggest that gravitational or hydrodynamic torques stemming from scales larger than the central regions play a fundamental role in transporting the necessary amount of gas to fuel the star formation in the central regions. How this is achieved physically and which processes are most important are some of the very important issues that will be investigated in a future study.

Second, the large inflows of gas in galaxies with or without major mergers produce compact, dense stellar cores/bulges with high velocity dispersions that are in agreement with observations and stable to bar formation. The dense massive stellar bulges significantly diminish the importance of the major mergers induced, additional gas inflows for galaxies at  $z \geq 1$ , in good agreement with earlier major mergers simulations of disk galaxies with massive bulges.

This result implies that a substantial revision of the current theoretical framework for galaxy formation is necessary, since some of the major foundational elements in our interpretation of galaxy properties hinge on the requirements/beliefs that major mergers are responsible for some of the extreme galaxy formation events, including high luminosity galaxies, such as starbursting galaxies, ULIRGs and SMGs, and formation of supermassive black holes.

Some additional results found that may also be interesting are:

- 10 – 20% of galaxies with stellar mass greater than  $10^{11} M_{\odot}$  are in major mergers at any time from  $z = 1 - 4$ .
- The merger rate per unit redshift is roughly constant at  $\sim 0.4$  for galaxies in the stellar mass range of  $10^{10.7} - 10^{11.7} M_{\odot}$  with an upturn and a dramatic downturn above and below that mass range, respectively, for the redshift range  $z \sim 1 - 4$ . A fitting formula is provided in Eq 1.
- For galaxies with SFR greater than  $200 M_{\odot}/\text{yr}$  we predict that about 10 – 40% should be seen in major mergers at  $z = 1 - 4$ . This predicted fraction is somewhat lower than what current spectral observations suggest (e.g., 57%; Tacconi et al. 2006) but can be directly tested with high resolution imaging with ALMA.
- It is predicted that the cumulative probability distribution function of major merging

galaxies within a projected separation  $r_p$  goes approximately as  $r_p^{1/4}$  for galaxies with  $\text{SFR} \geq 10 M_\odot/\text{yr}$  (for  $r_p$  greater than a few kpc). We expect that ALMA may be able to provide a direct measurement to test this.

Computing resources were in part provided by the NASA High- End Computing (HEC) Program through the NASA Advanced Supercomputing (NAS) Division at Ames Research Center. This work is supported in part by grants NAS8-03060 and NNX11AI23G.

## REFERENCES

- Abel, T., Anninos, P., Zhang, Y., & Norman, M. L. 1997, *New Astronomy*, 2, 181
- Bahcall, J. N., Kirhakos, S., Saxe, D. H., & Schneider, D. P. 1997, *ApJ*, 479, 642
- Barnes, J. E., & Hernquist, L. 1996, *ApJ*, 471, 115
- Bruzual, G., & Charlot, S. 2003, *MNRAS*, 344, 1000
- Bryan, G. L., & Norman, M. L. 1999, in *Structured Adaptive Mesh Refinement Grid Methods*, ed. N. P. C. S. B. Baden (IMA Volumes on Structured Adaptive Mesh Refinement Methods, No. 117), 165
- Buitrago, F., Trujillo, I., Conselice, C. J., Bouwens, R. J., Dickinson, M., & Yan, H. 2008, *ApJ*, 687, L61
- Cappellari, M., di Serego Alighieri, S., Cimatti, A., Daddi, E., Renzini, A., Kurk, J. D., Cassata, P., Dickinson, M., Franceschini, A., Mignoli, M., Pozzetti, L., Rodighiero, G., Rosati, P., & Zamorani, G. 2009, *ApJ*, 704, L34
- Cen, R. 2010, *ArXiv e-prints*
- . 2011a, *ApJ*, in press, arXiv1104.5046
- . 2011b, *ArXiv e-prints*
- Cen, R., Kang, H., Ostriker, J. P., & Ryu, D. 1995, *ApJ*, 451, 436
- Cen, R., Nagamine, K., & Ostriker, J. P. 2005, *ApJ*, 635, 86
- Cen, R., & Ostriker, J. P. 1992, *ApJ*, 399, L113
- Cimatti, A., Cassata, P., Pozzetti, L., Kurk, J., Mignoli, M., Renzini, A., Daddi, E., Bolzonella, M., Brusa, M., Rodighiero, G., Dickinson, M., Franceschini, A., Zamorani, G., Berta, S., Rosati, P., & Halliday, C. 2008, *A&A*, 482, 21

- Daddi, E., Renzini, A., Pirzkal, N., Cimatti, A., Malhotra, S., Stiavelli, M., Xu, C., Pasquali, A., Rhoads, J. E., Brusa, M., di Serego Alighieri, S., Ferguson, H. C., Koekemoer, A. M., Moustakas, L. A., Panagia, N., & Windhorst, R. A. 2005, *ApJ*, 626, 680
- Dalgarno, A., & McCray, R. A. 1972, *ARA&A*, 10, 375
- Di Matteo, T., Springel, V., & Hernquist, L. 2005, *Nature*, 433, 604
- Duc, P.-A., Mirabel, I. F., & Maza, J. 1997, *A&AS*, 124, 533
- Eisenstein, D., & Hu, P. 1999, *ApJ*, 511, 5
- Haardt, F., & Madau, P. 1996, *ApJ*, 461, 20
- Heckman, T. M. 2001, in *Astronomical Society of the Pacific Conference Series*, Vol. 240, *Gas and Galaxy Evolution*, ed. J. E. Hibbard, M. Rupen, & J. H. van Gorkom, 345
- Hopkins, P. F., Hernquist, L., Cox, T. J., Di Matteo, T., Robertson, B., & Springel, V. 2006, *ApJS*, 163, 1
- Joseph, R. D., & Wright, G. S. 1985, *MNRAS*, 214, 87
- Joung, M. R., Cen, R., & Bryan, G. L. 2009, *ApJ*, 692, L1
- Komatsu, E., Smith, K. M., Dunkley, J., Bennett, C. L., Gold, B., Hinshaw, G., Jarosik, N., Larson, D., Nolte, M. R., Page, L., Spergel, D. N., Halpern, M., Hill, R. S., Kogut, A., Limon, M., Meyer, S. S., Odegard, N., Tucker, G. S., Weiland, J. L., Wollack, E., & Wright, E. L. 2010, *ArXiv e-prints*
- Longhetti, M., Saracco, P., Severgnini, P., Della Ceca, R., Mannucci, F., Bender, R., Drory, N., Feulner, G., & Hopp, U. 2007, *MNRAS*, 374, 614
- Lowenthal, J. D., Koo, D. C., Guzman, R., Gallego, J., Phillips, A. C., Faber, S. M., Vogt, N. P., Illingworth, G. D., et al. 1997, *ApJ*, 481, 673
- Lutz, D., Spoon, H. W. W., Rigopoulou, D., Moorwood, A. F. M., & Genzel, R. 1998, *ApJ*, 505, L103
- Mihos, J. C., & Hernquist, L. 1996, *ApJ*, 464, 641
- Naab, T., Johansson, P. H., & Ostriker, J. P. 2009, *ApJ*, 699, L178
- Onodera, M., Daddi, E., Gobat, R., Cappellari, M., Arimoto, N., Renzini, A., Yamada, Y., McCracken, H. J., Mancini, C., Capak, P., Carollo, M., Cimatti, A., Giavalisco, M., Ilbert, O., Kong, X., Lilly, S., Motohara, K., Ohta, K., Sanders, D. B., Scoville, N., Tamura, N., & Taniguchi, Y. 2010, *ApJ*, 715, L6

- Ostriker, J. P., & Peebles, P. J. E. 1973, *ApJ*, 186, 467
- Sanders, D. B., Soifer, B. T., Elias, J. H., Madore, B. F., Matthews, K., Neugebauer, G., & Scoville, N. Z. 1988, *ApJ*, 325, 74
- Steidel, C. C., Adelberger, K. L., Adelberger, K. L., Shapley, A. E., Pettini, M., Dickinson, M., & Giavalisco, M. 2003, *ApJ*, 592, 728
- Steinmetz, M., & White, S. D. M. 1997, *MNRAS*, 288, 545
- Tacconi, L. J., Neri, R., Chapman, S. C., Genzel, R., Smail, I., Ivison, R. J., Bertoldi, F., Blain, A., Cox, P., Greve, T., & Omont, A. 2006, *ApJ*, 640, 228
- Toft, S., van Dokkum, P., Franx, M., Labbe, I., Förster Schreiber, N. M., Wuyts, S., Webb, T., Rudnick, G., Zirm, A., Kriek, M., van der Werf, P., Blakeslee, J. P., Illingworth, G., Rix, H., Papovich, C., & Moorwood, A. 2007, *ApJ*, 671, 285
- Toomre, A., & Toomre, J. 1972, *ApJ*, 178, 623
- Trujillo, I., Feulner, G., Goranova, Y., Hopp, U., Longhetti, M., Saracco, P., Bender, R., Braitto, V., Della Ceca, R., Drory, N., Mannucci, F., & Severgnini, P. 2006a, *MNRAS*, 373, L36
- Trujillo, I., Förster Schreiber, N. M., Rudnick, G., Barden, M., Franx, M., Rix, H., Caldwell, J. A. R., McIntosh, D. H., Toft, S., Häussler, B., Zirm, A., van Dokkum, P. G., Labbé, I., Moorwood, A., Röttgering, H., van der Wel, A., van der Werf, P., & van Starkenburg, L. 2006b, *ApJ*, 650, 18
- van de Sande, J., Kriek, M., Franx, M., van Dokkum, P. G., Bezanson, R., Whitaker, K. E., Brammer, G., Labbé, I., Groot, P. J., & Kaper, L. 2011, *ApJ*, 736, L9+
- van Dokkum, P. G., Kriek, M., & Franx, M. 2009, *Nature*, 460, 717